Lawrence Berkeley National Laboratory

Title
Design Study of the Extraction System of the 3rd Generation ECR Ion Source

Permalink
https://escholarship.org/uc/item/0p84987m

Author
Wutte, D.

Publication Date
1998

ERNEST ORLANDO LAWRENCE BERKELEY NATIONAL LABORATORY

Design Study of the Extraction System of the 3rd Generation ECR Ion Source

D. Wutte, M.A. Leitner, C.M. Lyneis,
C.E. Taylor, and Z.Q. Xie

Nuclear Science Division

DISCLAIMER

Design Study of the Extraction System of the
3rd Generation ECR Ion Source

D. Wutte, M.A. Leitner, C.M. Lyneis, C.E. Taylor, and Z.Q. Xie

Nuclear Science Division
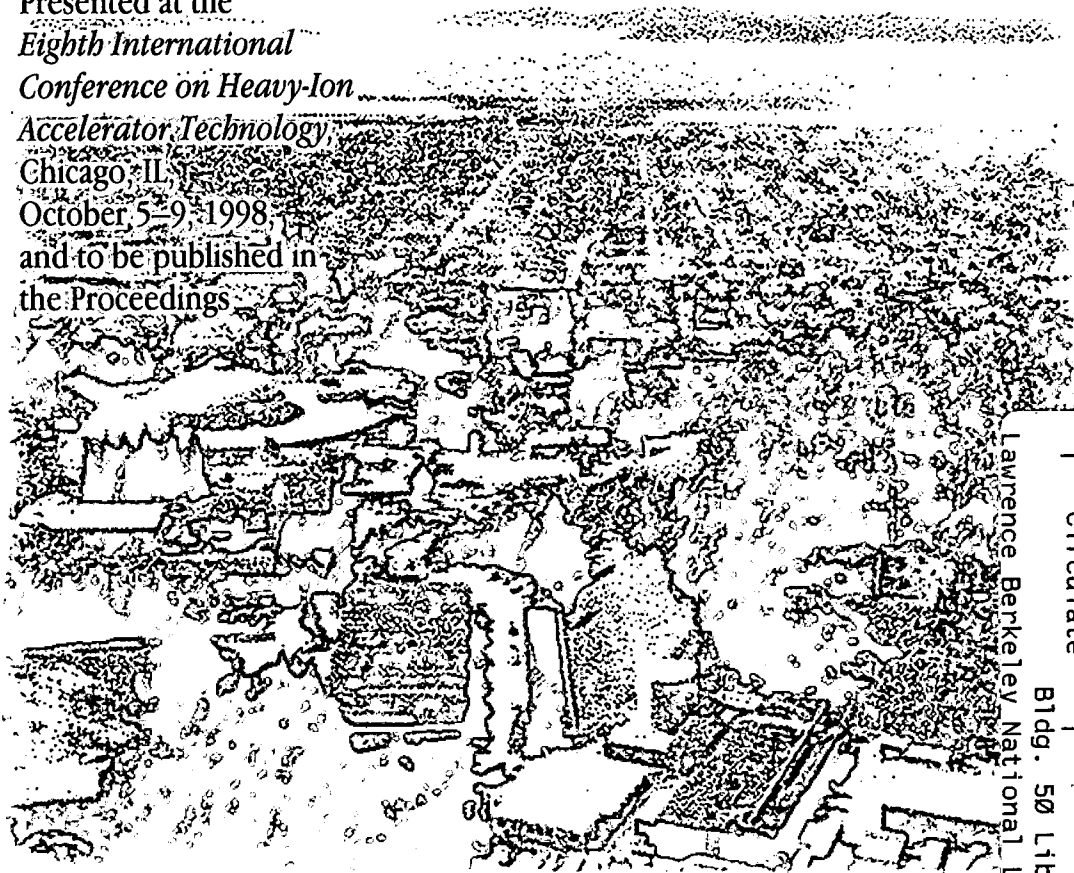Ernest Orlando Lawrence Berkeley National Laboratory
University of California
Berkeley, California 94720

October 1998

Design Study of the extraction system of the 3rd Generation ECR ion source

D. Wutte, M. A. Leitner, C. M. Lyneis, C. E. Taylor, Z. Q. Xie

Ernest Orlando Berkeley National Laboratory, University of California at Berkeley
Berkeley, California 94720, USA

Abstract. A design study for the extraction system of the 3rd Generation super conducting ECR ion source at LBNL is presented. The magnetic design of the ion source has a mirror field of 4 T at the injection and 3 T at the extraction side and a radial field of 2.4 T at the plasma chamber wall. Therefore, the ion beam formation takes place in a strong axial magnetic field. Furthermore the axial field drops from 3 T to 0.4 T within the first 30 cm. The influence of the high magnetic field on the ion beam extraction and matching to the beam line is investigated. The extraction system is first simulated with the 2D ion trajectory code IGUN with an estimated mean charge state of the extracted ion beam. These results are then compared with the 2D code AXCEL-INP, which can simulate the extraction of ions with different charge states. Finally, the influence of the strong magnetic hexapole field is studied with the three dimensional ion optics code KOBRA. The introduced tool set can be used to optimize the extraction system of the super conducting ECR ion source.

INTRODUCTION

With the construction of the LBNL 3rd Generation ECR ion source we expect to further enhance the performance of the 88" cyclotron by providing more intense highly charged heavy-ion beams (1). Record high charge states and beam intensities are provided by the AECR-U ion source (2) and usable beams for elements up to mass 200 can be extracted from the cyclotron with sufficient intensities for nuclear structure experiments such as Gammasphere (3). However, for low cross section experiments with the Berkeley Gas-filled Spectrometer (BGS) now coming on line at the 88" cyclotron higher ion beam intensities will be required. With the third Generation ECR ion source we will increase both the maximum charge states and beam intensities for the science programs at the 88" Cyclotron facility.

The magnetic design of the third Generation ECR ion source has a maximum axial field of 4 Tesla at the injection side and 3 Tesla at the extraction side. The maximum hexapole field is 2.4 Tesla at the plasma chamber wall. Figure 1 shows the ion source layout and Figure 2 shows the axial field at full coil excitation. Due to the size of the superconducting coils, the distance from the plasma outlet aperture to the exit of the iron shielding yoke it is about 30 cm. At full coil excitation the axial magnetic field drops from 3 T to 0.4 T within this distance. The axial magnetic field then drops further below 20 G within the next 30 cm. Therefore, the beam formation takes place in a strong magnetic field and has to be included in the ion optics layout.
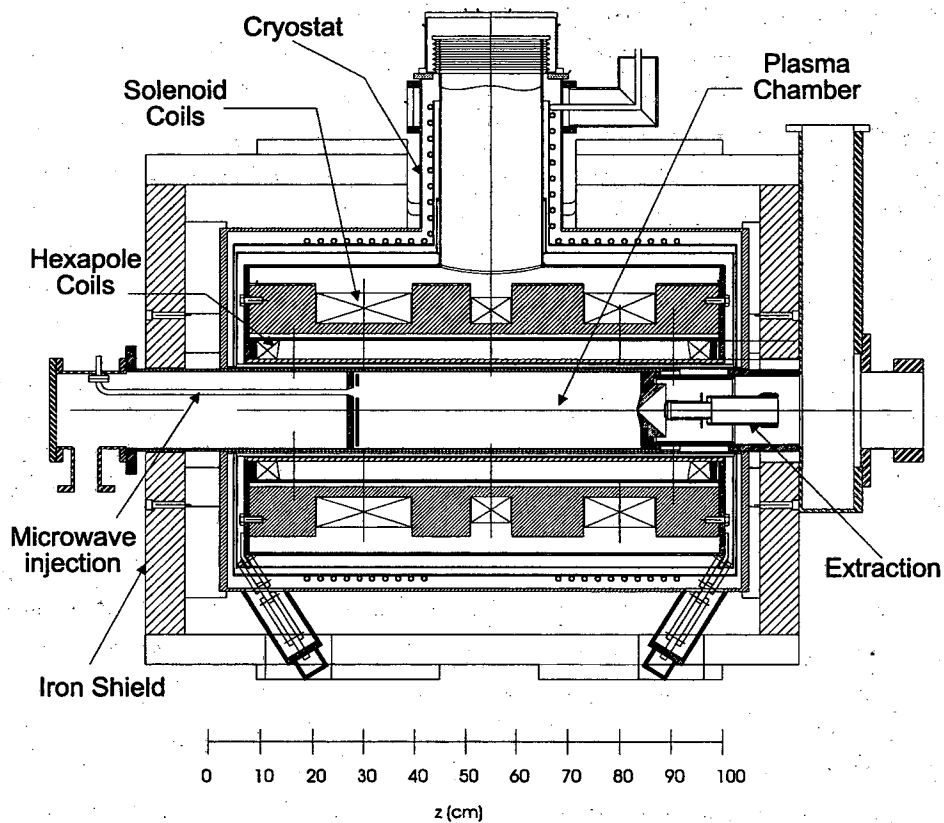
Figure 1. Mechanical layout for the LBNL 3rd Generation ECR ion source, including the iron shield, cryostat, coils, and plasma chamber.
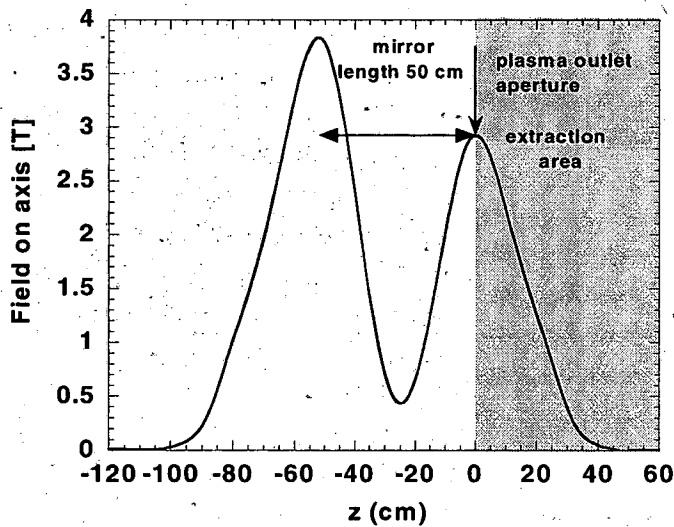
Figure 2. Axial magnet field of the LBNL 3rd Generation ECR ion source.

2

EXTRACTION SIMULATION OF MULTIPLY CHARGED ION BEAMS IN THE PRESENCE OF STRONG MAGNETIC FIELDS

During the optimization process of an extraction and beam transport system, it is more convenient to simulate only one charge state. It is then possible to concentrate on the transmission of the charge state of interest. Furthermore, computer capacity limits the maximum number of simulated particle trajectories, which can be simulated in reasonable times. By using only one charge state (compared to 20 in the case of argon with oxygen mixing gas) many more particle trajectories can be allocated to the charge state of interest. For these reasons the ion optics code IGUN (4) is used for our first design study. We introduce a physical approximation, which models the extraction of many charge states from an ECR ion source by using only a single charge state. We will compare the IGUN results with AXCEL-INP (5) simulations. AXCEL can simulate the extraction of different charge states simultaneously. Both computer codes use a one-dimensional plasma sheath model and can import axial magnetic field tables.

In the first part of the paper, we describe our model. The second part presents simulation results:

1. IGUN simulations for the extraction gap (2D)
2. Comparison of the IGUN results with AXCEL runs (2D)
3. Influence of the hexapole field on the ion optics (3D)

Finally, we describe the preliminary beam line layout to a Faraday cup after the bending magnet. In that way we are establishing a tool set for further extraction and beam line optimization of the 3rd Generation ECR ion source.

Simulation model

Since IGUN can only simulate one charge state, we will approximate the extraction of many charge states from an ECR ion source by considering only one charge state. It is incorrect to model the beam transport by using the mean charge state (weighted by the current of each charge state). Such a simplification is unphysical, because it does not model the plasma sheath correctly nor the space charge allocation along the beam path. Furthermore, it is not possible to simulate the influence of the magnetic field on the beam envelope for different charge states (see Figure 4). In the strong magnetic field, different charge states have different focal lengths and emittance orientations in phase space (Figure 7). For instance if we calculate the example charge state distribution for Ar^{16+} (Table 1) with a mean mass-to-charge of 12.44, it will result in an emittance pattern within the 20 different emittance pattern for the whole ensemble (see Figure 7). Therefore, no prediction can be made for a particular charge

3

state. The mean charge state approach would give incorrect simulation results and would lead to an non-optimized design.

For our simulations, we have normalized the current of each charge state of each ion to the equivalent current for the charge state of interest by using the Child-Langmuir relation

$$j = 1.72 \cdot \frac{U^{3/2}}{d^2} \sqrt{\frac{q}{M}} \, ,$$ (1)

with j is the current density in (mA/cm²), q is the charge state, M is the ion mass (amu), U is the extraction voltage (kV), d is the extraction gap width (cm).

The Child-Langmuir relation calculates the maximum extractable current under space charge limited conditions from a plasma for a plane meniscus, which is proportional to $\sqrt{q/m}$. To obtain the same plasma sheath conditions (e.g. a straight plasma sheath at a given extraction voltage) more current must be extracted for the higher charge states q/m than for the lower ones. The procedure of computing the different current contributions of a CSD must consider this behavior. Therefore, we will normalize the contribution of each single charge state q/m of the CSD by multiplying with $\sqrt{m/q} \cdot \sqrt{Q/M}$. Q/M corresponds to the charge state of interest, which will be simulated in the computer model. This approach models the plasma sheath position correctly with only a single charge state and a normalized current value, which includes the current contributions of all the other charge states. In particular, the ion-optical magnetic field influence on the charge state of interest is modeled accurately. Furthermore, the space charge allocation along the beam path is accurate as long as the overall beam envelope does not change considerably. The extraction system can now be optimized for a chosen charge state and plasma condition without including explicitly all the other charge states.

If we want to simulate the transport of an Ar^{16+} ion beam, each charge state of the CSD has to be normalized to Ar^{16+} according to

$$I_{Ar^{n+}_{equivalent}} = I_{Ar^{m+}} \cdot \sqrt{\left(\frac{n}{m}\right)},$$ (2)

n and m are argon charge states, $I_{Ar}m+$ is the current to be normalized.

For example for the charge state Ar^{10+} with $I_{Ar^{10+}} = 64e\mu A$ the normalized Ar^{16+} current would be $I_{Ar^{16+}_{equivalent}} = 81e\mu A$. For the correct simulation of a high charge state distribution, we have included the charge state distribution of the oxygen mixing gas. In that case, the oxygen currents have to be converted to Ar-equivalent currents in the following way

$$I_{Ar^{n+}_{equivalent}} = I_{O^{q+}} \cdot \sqrt{\left(\frac{n}{q}\right)} \sqrt{\left(\frac{M_O}{M_{Ar}}\right)} \quad \text{with } \frac{M_O}{M_{Ar}} = \frac{16}{40} .$$ (3)

INPUT PARAMETERS

As an example, we have modeled two different charge state distributions (CSD) for argon; a high-current medium charge state distribution optimized for Ar^{9+} and a lower- current high-charge state distribution optimized for Ar^{16+} as extracted from the AECR-U. Table 1 summarizes the CSDs as used in the simulations with the ion optics codes ACXEL and IGUN. The axial magnetic fields were calculated with TOSCA3D and imported into the ion trajectory codes.

TABLE 1. A high-current medium charge-state distribution optimized for Ar^{9+} and a lower-current charge-state distribution optimized for Ar^{16+} . For IGUN simulations the total Ar^{9+} or Ar^{16+} equivalent current (indicated by the Σ sign) has been used as input parameter. For AXCEL simulations, each charge state and electrical current have been used as input parameters.

input ion beam distributions						
CSD optimized for Ar $^{9+}$			CSD optimized for Ar $^{16+}$ with oxygen gas mixing			
q	CSD* [eμA]	Ar $^{9+}$ equiv. curr. [eμA]	CSD* [eμA]	Ar $^{16+}$ equiv. curr. [eμA]	O$_2$ CSD* [eμA]	O^{n+}, equiv. curr. [eμA]
16	0.48	0.36	17	17		
15	3.2	2.5	45	46		
14	13.3	10.7	69	74		
13	43	36	78	86		
12	107	93	85	98		
11	217	196	75	90		
10	385	365	64	81		
9	483	483	57	76		
8	502	532	50	71		
7	231	262	49	74	48	46
6	183	225	45	73	97	100
5	207	277	40	72	80	91
4	100	150	38	76	72	91
3	100	173	35	81	70	102
2	80	170	30	85	70	125
1	60	180	25	100	70	177
Σ eμA	2715	3156	802	1200	507	732

*typical AECR-U CSD, corrected for transport losses (current estimates were made for the lower charge states below Ar^{5+})

SIMULATION RESULTS
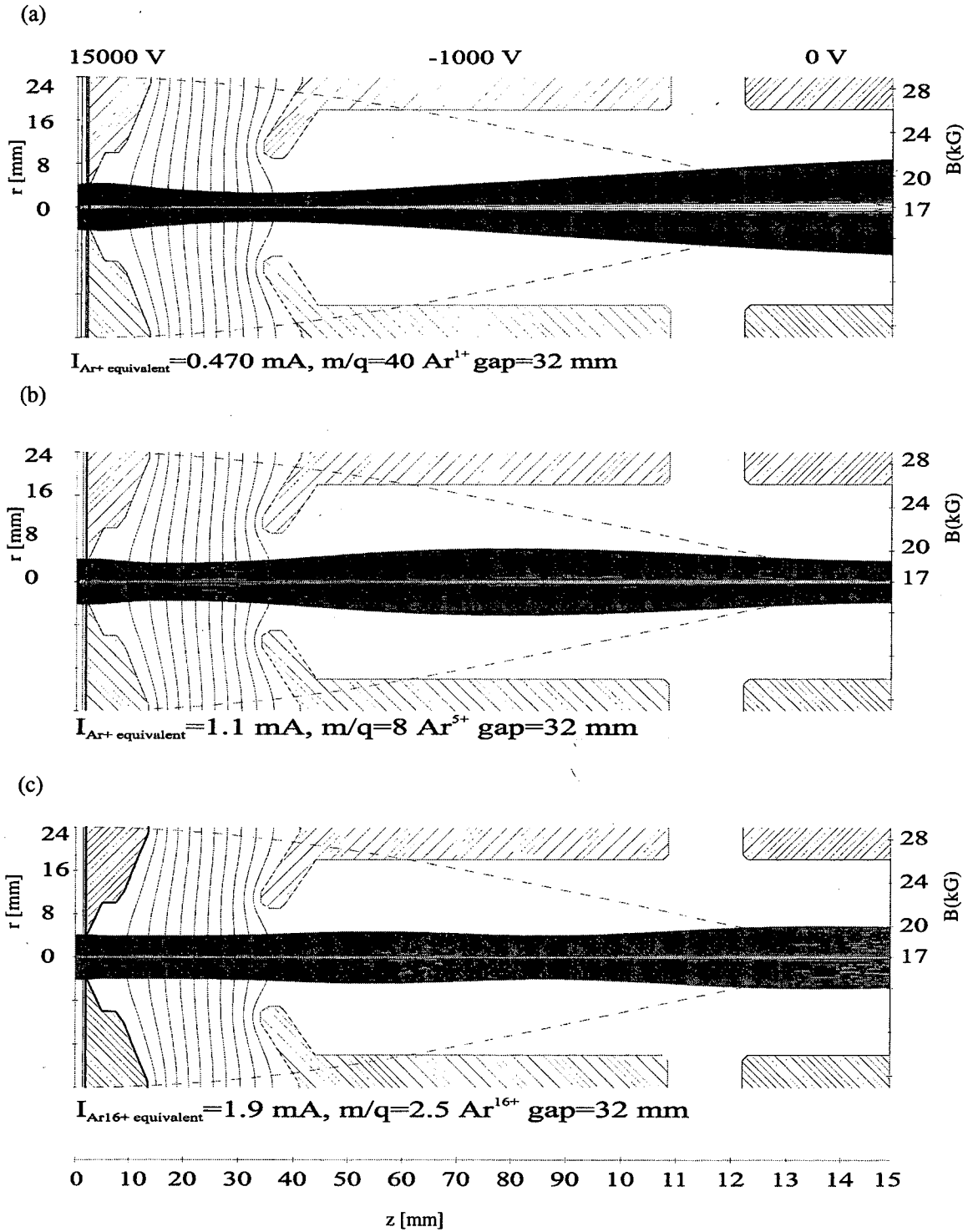
Extraction system layout

Figure 4 shows the layout for the extraction system. The recess in the plasma outlet aperture creates a more uniform electric field equipotential surface at the plasma meniscus (Figure 3). The aperture edge thickness has been chosen as small as practically feasible (e.g. a 0.2mm thickness is a practical value, especially when plasma heat load problems are considered). Generally the thinner the edge of the plasma outlet aperture the smaller are the ion beam losses to the outlet electrode, resulting in a higher extractable ion current at a given plasma density. This behavior is demonstrated in figure 3 with a thick (figure 3a) and a thin (figure 3b) plasma outlet aperture. In the case of a 3 mm thick electrode about 47% of the outward directed current is lost to the electrode. Furthermore the electric equipotential contour lines are less distorted for the thin edge and fewer aberrations are induced to the ion beam (7).
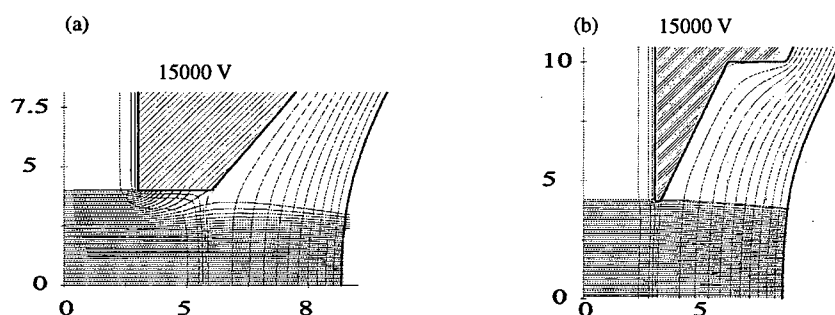
Figure 3.   Equipotential contour lines computed at the plasma sheath for a thick (3 mm, figure2a) and a thin (0.2 mm, figure2b) plasma electrode. In both simulations, the distance between the accel electrode and the plasma outlet aperture was 29mm. The density has been adjusted to maintain a flat plasma sheath. In case (a) the total extracted current was 1.5 mA; about 47 % of the available current gets lost in the extraction hole. In case (b) the total extracted current was 3 mA.

Figure 4 shows the influence of the magnetic field on the ion beams of Ar^{1+}, Ar^{5+}, and Ar^{16+}. The equivalent currents for Ar^{1+} (a), Ar^{5+} (b), and Ar^{16+} (c) were computed according to equation 1 and 2 for the lower current CSD (optimized for Ar^{16+}). Each charge state has a different beam envelope in the strong axial magnetic field. For example the waist of Ar^+ is further downstream than for Ar^{16+}. Therefore, the singly charged Ar beam is strongly divergent (Figure 4a) at z = 15 cm, whereas Ar^{16+} is convergent (Figure4c).

Figure 5 shows how the location of the rms Ar^{16+} emittance ellipse in phase space can be optimized when the extraction gap spacing is changed. In that way it is possible to match the ion beam extraction to the beam line. Considering the wide range of plasma conditions of this ECR ion source, a movable extraction system will be essential for tuning the beam transport.

(a)

15000 V   -1000 V   0 V

$I_{Ar+ \, equivalent}$=0.470 mA, m/q=40 Ar^{1+} gap=32 mm

(b)

$I_{Ar+ \, equivalent}$=1.1 mA, m/q=8 Ar^{5+} gap=32 mm

(c)

$I_{Ar16+ \, equivalent}$=1.9 mA, m/q=2.5 Ar^{16+} gap=32 mm

Figure 4.   Influence of the magnetic field on the ion beams of Ar^{1+}, Ar^{5+}, and Ar^{16+} as computed with IGUN for the low current CSD (see Table 1).

7

The lowest emittance for Ar^{16+} has been calculated for an extraction gap of 32 mm. The calculated 100 % rr' normalized emittances for this case are 0.108 π mm mrad for an thermal ion energy spread of 0.1 eV and 0.289 π mm mrad for an thermal ion energy spread of 3 eV.
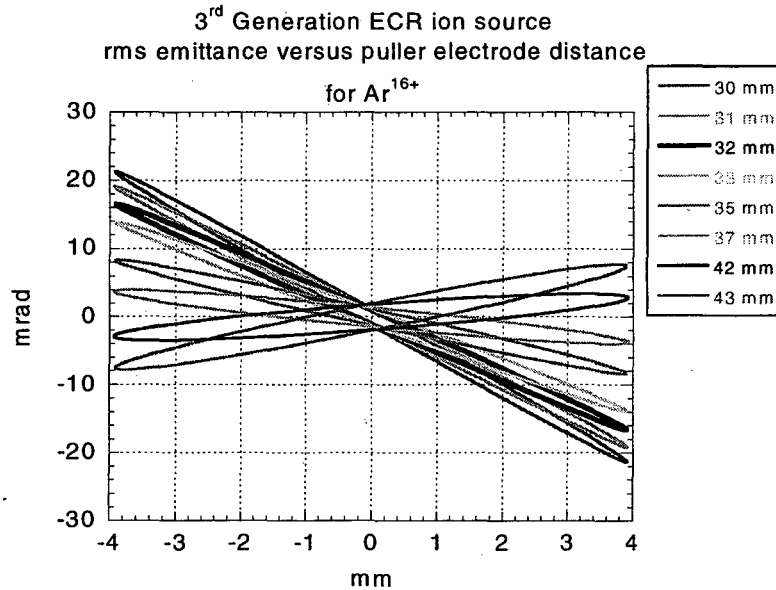

Figure 5. Change of the rms emittance figure versus the distance between the accel-decel system and the plasma outlet aperture for an Ar^{16+} ion beam. The black ellipse indicates the distance with lowest rms emittance for these particular plasma conditions.

Comparison between IGUN and AXCEL simulations

We have compared the simulation results for IGUN and AXCEL at the same input condition. Figure 6 shows the output emittances for both programs for the extraction system as described in Figure 4; the results are in good agreement.

To validate our approach of using a single charge state for the extraction system optimization, we calculated the complete charge state distribution for both CSD as described in Table 1 with AXCEL-INP.

As an example the emittance patterns for all different argon and oxygen charge states for the Ar^{16+} sample CSD is shown in Figure 7. The different focal length for each charge state can be clearly seen.
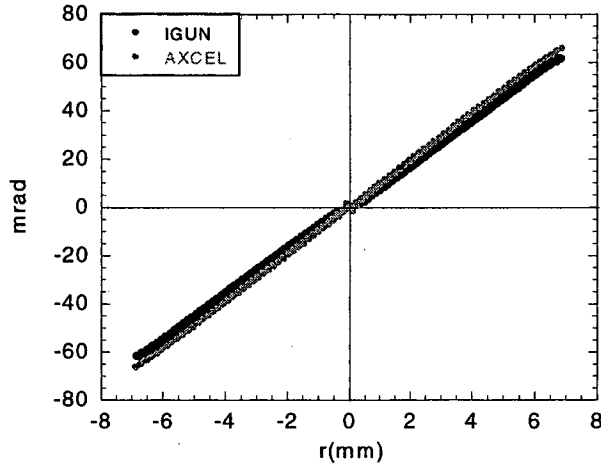
**Figure 6.** Comparison of an IGUN simulation and with an AXCEL simulation at the same input conditions m/q=4.4444, I_{extr} = 3.1 emA, the 100% normalized rr' emittance is about 0.32 π mm mrad.

As an example the emittance patterns for all different argon and oxygen charge states for the Ar^{16+} sample CSD is shown in Figure 7. The different focal length for each charge state can be clearly seen.
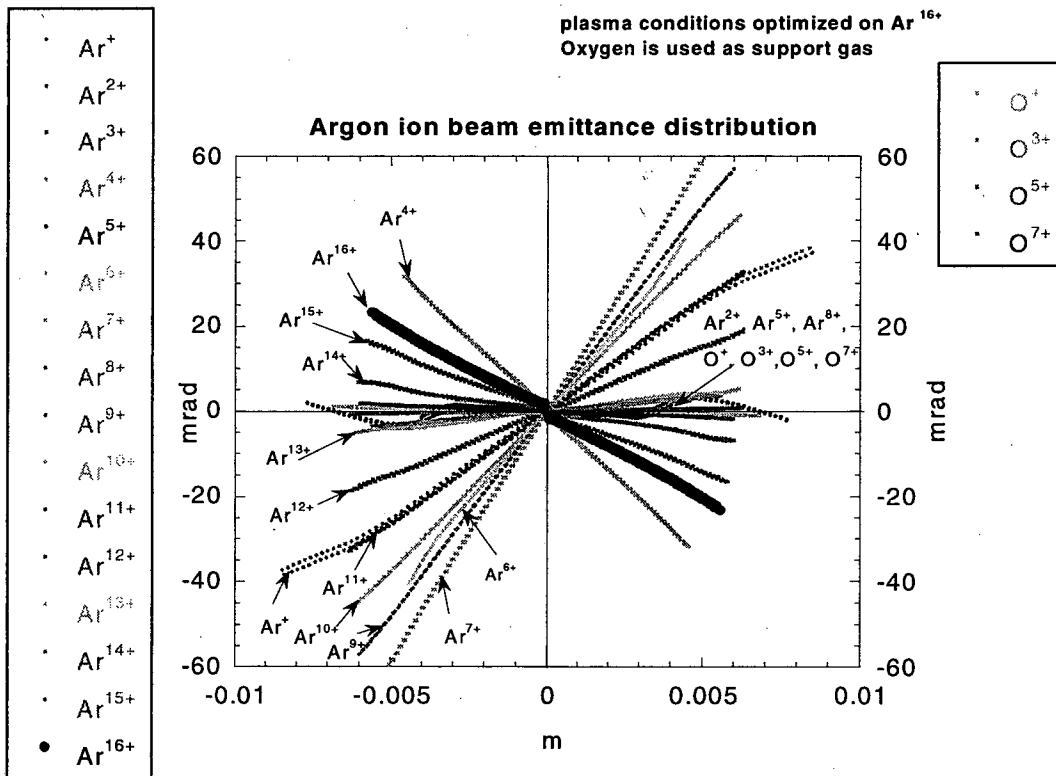
Figure 7. Emittance pattern as calculated with AXCEL. The different charge states are shaded in gray. Ar^{16+} is drawn in black.

9

We simulated different argon charge states for the low current-medium CSD by using the current equivalent method with IGUN. Figure 8 compares the emittance pattern, the agreement with AXCEL-INP results (considering all charge states, see Figure7) is remarkable. Figure 8b shows this comparison for the high current-medium CSD for Ar^{9+}.
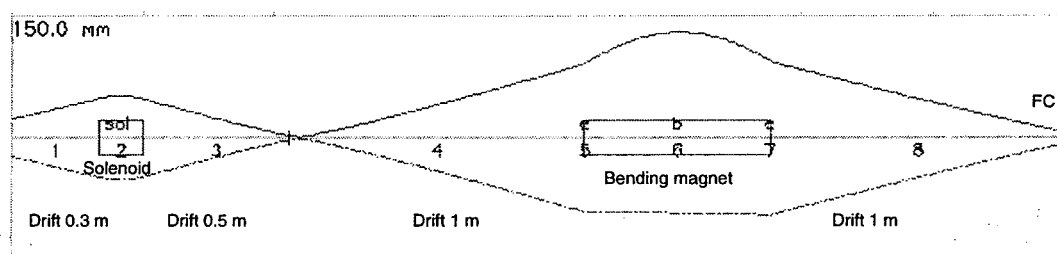

3rd Generation ECR ion source
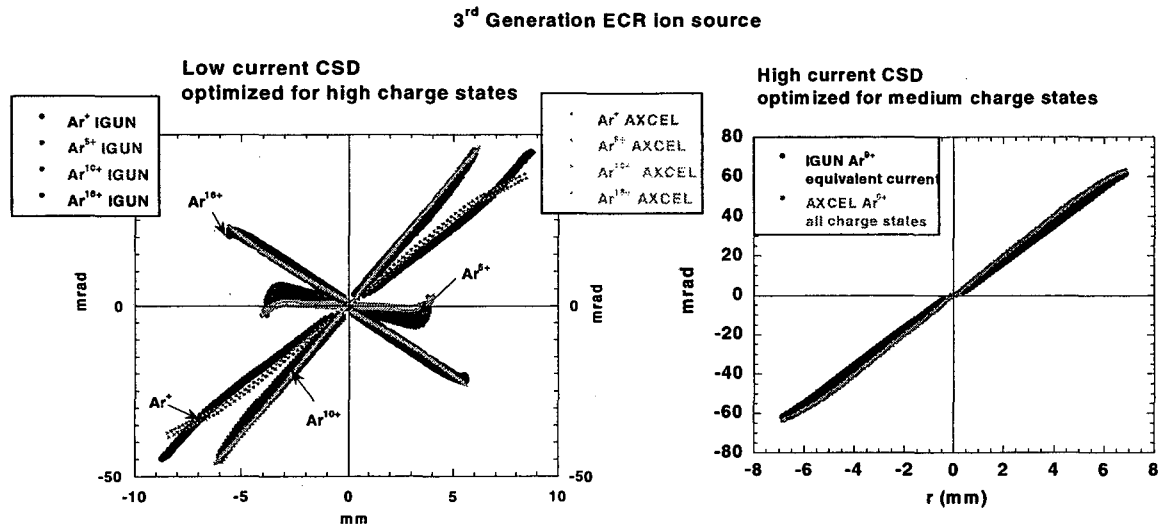
Figure 8. Comparison of the Ar^{16+} emittance pattern from (Figure7) of the AXCEL simulation (considering all charge states) with the IGUN calculation for Ar^{1+}, Ar^{5+}, Ar^{10+}, and Ar^{16+} (equivalent current methode). Figure 8b shows the same comparison for the high current medium charge state distribution. Both simulation result in the same rr' emittance.

Influence of the sextupole field

The influence of the magnetic hexapole field has been studied with the three dimensional ion optics code KOBRA (5). The magnetic input data table has been calculated with TOSCA. The influence of the hexapole field has been found to be negligible. This result is not surprising since the hexapole field strength at 1cm diameter (extraction aperture ⌀8mm) does not exceed 150 G. Of course only the influence on the ion optics has been investigated. We have not included any variation of the ion current density across the plasma electrode orifice (caused by plasma density variations due to the magnet field structure).

BEAM LINE

A first layout of the beam line from the 3rd Generation ECR ion source to the Faraday cup after the bending magnet is shown in Figure 9, calculated with TRACE2D (7). The design has a Glazer lens (0.60 m downstream from the plasma outlet aperture) and a double focusing sector magnet (2.4 m downstream from the plasma outlet aperture). The first 30 cm have been calculated with IGUN for Ar^{9+} with an equivalent current for the high current-medium CSD beam (Table 1). The output beam parameter from IGUN at z = 30 cm have been used as input parameter for TRACE 2D. By combining these two computer codes we are able to consistently simulate the beam from the plasma meniscus through the beam line.

Figure 9.   Preliminary layout of the beam line from the 3rd Generation ECR ion source to the Faraday cup after the bending magnet.

CONCLUSION

A tool set for optimizing the extraction system of an ECR ion source in the presence of a strong magnetic field has been introduced. It has been shown that the beam formation of a particular charge state can be modeled by normalizing the charge state current distribution to an equivalent current. A first layout for the extraction system and the ion beam transport line has been presented.

ACKNOWLEDGMENT

11

REFERENCES

(1)   C. M. Lyneis, Z. Q. Xie, C. E. Taylor, Rev. of Scientific Instruments **69**, 682 (1998)

(2)   Z.Q. Xie, Rev. Sci. Instrum. **69**, 625 (1998)

(3)   C. M. Lyneis, Z. Q. Xie, D. J. Clark, Proceedings of the 14th International Conference on Cyclotrons and their Applications, Cape Town, S. Africa, Oct. 8-13, 1995

(4)   R. Becker, W. B. Hermannsfeldt, RSI **63**, 2756 (1991)

(5)   INP, Junkernstr. 99, 65205 Wiesbaden, Germany; http://www.inp-dme.com/

(6)   J. R. Coupland, T. S. Green, D. P. Hammond, A. C. Riviere, Rev. Sci. Instrum **44** (1973)

(7)   TRACE3D Documentation, K. R. Crandall, D. P. Rusthoi, LA-UR-97-886, Los Alamos National Laboratory Report, May 1997